

MATERIALS SCIENCE

Correlated insulating and superconducting states in twisted bilayer graphene below the magic angle

Emilio Codecido¹, Qiyue Wang², Ryan Koester¹, Shi Che¹, Haidong Tian¹, Rui Lv¹, Son Tran¹, Kenji Watanabe³, Takashi Taniguchi³, Fan Zhang^{2*}, Marc Bockrath^{1*}, Chun Ning Lau^{1*}

The emergence of flat bands and correlated behaviors in “magic angle” twisted bilayer graphene (tBLG) has sparked tremendous interest, though its many aspects are under intense debate. Here we report observation of both superconductivity and the Mott-like insulating state in a tBLG device with a twist angle of $\sim 0.93^\circ$, which is smaller than the magic angle by 15%. At an electron concentration of ± 5 electrons/moiré unit cell, we observe a narrow resistance peak with an activation energy gap ~ 0.1 meV. This indicates additional correlated insulating state, and is consistent with theory predicting a high-energy flat band. At doping of ± 12 electrons/moiré unit cell we observe resistance peaks arising from the Dirac points in the spectrum. Our results reveal that the “magic” range of tBLG is in fact larger than what is previously expected, and provide a wealth of new information to help decipher the strongly correlated phenomena observed in tBLG.

INTRODUCTION

Twistronics (1–7), the use of the relative twist angle between adjacent van der Waals layers to produce a moiré superlattice and flat bands, has emerged as a new and uniquely suitable approach to markedly alter and tailor the properties of devices based on two-dimensional materials. The marked effect of twistronics is exemplified by the recent groundbreaking works that demonstrated the emergence of extremely flat bands when two monolayer graphene layers are stacked at a “magic” twist angle, $\theta = 1.1 \pm 0.1^\circ$ (8, 9). In these twisted bilayer graphene (tBLG) devices at the magic angle, an insulating phase is observed at half filling of the superlattice’s first miniband, identified to be a Mott-like insulator, and superconductivity at slightly higher and lower doping. The phase diagram is reminiscent of high-temperature superconductors (10) for the high ratio between the superconducting transition temperature T_c to the Fermi temperature T_F , the relatively small Fermi surface, and the vicinity of the superconducting phase to an insulating state with an apparent magnetic ordering (9). These works have immediately sparked tremendous interest and ignited intense theoretical debate on nearly every aspect of this system, including low-energy band structure, band topology, irreducible symmetries, nature of the correlated insulating state, pairing mechanism and symmetry of the superconducting phase, the exact phase diagram, and additional magic angles (11–35). In contrast, apart from the initial reports, experimental studies are scarce and just starting to emerge (35–39).

Here, we report transport measurements of a magic angle tBLG device that exhibits both correlated insulating and superconducting states. Unexpectedly, the twist angle is measured to be $0.93^\circ \pm 0.01^\circ$, which is 15% smaller than the already established magic angles (7–9) and is the smallest reported to date that exhibits superconductivity. A correlated insulating state is observed at half filling $n_m = 2$, where n_m is the number of charges per moiré unit cell, and superconductivity at $n_m \approx 2.7$. Extending measurements to carrier densities $|n_m| > 4$, we observe previously unreported, narrow resistance peaks at $n_m = \pm 5$, each of which displays an activation gap of ~ 0.1 meV. This behavior is consistent with

the emergence of additional correlated insulating states when the next electron or hole band beyond the low-energy moiré Dirac bands is quarter-filled. Theoretical calculations indicate that these two high-energy bands have energetically flat regions in the moiré Brillouin zone with substantially large densities of states (DOS). Prominent resistance peaks also appear at $n_m = \pm 12$, which can be accounted for by the existence of a pair of Dirac points in the high-energy spectrum. Our results indicate that new correlated states can emerge in tBLG below the primary magic angle and beyond the first miniband, provided that the bands are sufficiently flat.

RESULTS AND DISCUSSION

Devices are fabricated using the “tear and stack” approach, encapsulated between hexagonal BN layers (8, 9), patterned into a Hall bar geometry with multiple leads, and coupled to Cr/Au edge contacts (40). The entire device is fabricated on top of a graphite layer that serves as the back gate [e.g., see (41)]. Figure 1 (A and B) shows a schematic diagram of the layer stack and the moiré superlattice, respectively. The devices are then measured in pumped He⁴ and He³ cryostats using standard dc and ac lock-in techniques.

Figure 1C displays the device’s longitudinal resistance R_{xx} versus an extended gate voltage V_g range and magnetic field B at a temperature $T = 1.7$ K, while the inset to Fig. 1D shows an optical image of the device. The main resistance peak at $V_g = 0$ corresponds to the charge neutrality point with $n_m = 0$. From the Landau fan emanating from $V_g = B = 0$, we find the back gate capacitance to be $C_b = 374$ nF/cm². Notably, two additional prominent peaks appear at $V_g = 0.83$ V and $V_g = -0.87$ V, each accompanied by a set of Landau fans. The small electron-hole asymmetry may be intrinsic to tBLG and has been observed in previous reports (8, 9). We therefore take the features at $V_g = \pm 0.85$ V as the satellite peaks that occur when the low-energy moiré bands are filled at densities $n_m = \pm 4$ (8, 9). Covering an unprecedentedly large range of carrier density up to $n_m = \pm 14$, the data exhibit Landau fans that converge to $n_m = 4m$, where m is an integer. Given the spin and valley degeneracies in graphene, this is consistent with the Wannier theory (42) that generally predicts that spectral gaps in the Hofstadter butterfly for spinless electrons in a single band follow the Diophantine equation $n_m = t\phi/\phi_0 + s$, where s and t are integers, ϕ is the flux per moiré unit cell, and ϕ_0 is the flux quantum. Using $4n_0 \approx \frac{80^2}{\sqrt{3}a^2}$,

¹Department of Physics, The Ohio State University, Columbus, OH 43210, USA.²Department of Physics, The University of Texas at Dallas, Richardson, TX 75080, USA.³National Institute for Materials Science, 1-1 Namiki, Tsukuba, Ibaraki 305-0044, Japan.

*Corresponding author. Email: zhang@utdallas.edu (F.Z.); bockrath.31@osu.edu (M.B.); lau.232@osu.edu (C.N.L.)

where $a = 0.246$ nm is the lattice constant of graphene and n_0 is the average density corresponding to $n_m = 1$, we estimate that $\theta = 0.93^\circ$, which corresponds to a moiré unit cell area A of 200 nm² and moiré lattice constant of 15.2 nm. We note that this is the smallest twist angle value reported to date for tBLG devices exhibiting superconductivity.

A close examination of the Landau fan in Fig. 1C reveals a number of salient features. We first focus on the low- to moderate-density regime, where $|n_m| < 4$. At $V_g = 0.43$ V or $n_m = +2$, a resistance peak appears, from which an accompanying set of Landau levels emanates, with a degeneracy of two. This peak at half filling and the twofold degeneracy of Landau levels is consistent with the previous observation of a Mott-like correlated insulating state (8). They indicate the breaking of approximate spin-valley SU(4) symmetry and the formation of a new quasi-particle Fermi surface, although the details require more delicate examination. Figure 1D displays $R_{xx}(V_g)$ at $B = 0$ and T ranging from 5.2 K down to 0.28 K, where the resistance peaks at $n_m = 0, \pm 4$, and ± 2 are visible. At $T = 280$ mK, for $0.51 < V_g < 0.65$ or, equivalently, $2.4 < n_m < 3.1$, R_{xx} is zero within our measurement error, indicating the emergence of superconductivity (9). This emergence of superconductivity and possibly percolating superconducting regions may be responsible for the increasing R_{xx} with increasing T at $n_m = 2$, similar to that observed in (9).

To determine the critical temperature T_c of the superconducting phase, we measure $\rho(T)$ at $V_g = 0.53$ V or $n_m \approx 2.5$ (Fig. 2A). As T decreases, ρ drops to zero, undergoing two successive steep descents

at $T \sim 1.5$ and $T \sim 0.3$ K. Such a two-step transition has been observed in other magic angle tBLG device (36) and may be related to non-Planckian dissipation of the strange metal state. Alternatively, it may arise from spatial or structural inhomogeneity of our device or from the presence of domains that host competing superconducting states of different pairing symmetries and critical temperatures. We note that these data were not taken at optimal doping for superconductivity in this sample, and T_c could be as high as ~ 0.5 K. However, the device became nonfunctional before clear data could be obtained.

To further investigate the superconducting phase, we measure the device's four-terminal voltage-current (V - I) characteristics at different carrier densities. Figure 2B displays resistance, which is obtained by numerically differentiating the V - I curves, as a function of V_g and bias current I . V - I characteristics at two representative densities, $V_g = 0.50$ V and $V = 0.58$ V, are shown in Fig. 2C. Supercurrent is observed for an extended range of density, with critical current I_c ranging from ~ 1 to 15 nA; at $V_g \sim 0.58$ V, the maximum value of I_c is observed. We therefore take $V_g \sim 0.58$ V (or $n_m \sim 2.7$) to be the optimal doping. Upon application of a parallel magnetic field H , the supercurrent is suppressed, with a critical field of $H_{||c} \sim 0.5$ T (Fig. 2D), consistent with previous work (9).

To gain insight into this behavior, we calculate the moiré band structure for the 0.93° tBLG using the Bistritzer-MacDonald model (7) with refined parameter values that take into account lattice relaxation: $t_{AA} = 79.7$ meV, $t_{AB} = 97.5$ meV, and $v_F = 7.98 \times 10^5$ m/s (43). Here, t_{AA} and t_{AB} are the electron interlayer tunneling amplitudes between the same and different sublattices, respectively, and v_F is the Fermi velocity. In sharp contrast to those cases near and above the magic angle, our calculation of the 0.93° tBLG shows that the low-energy moiré Dirac bands ($|n_m| < 4$) are not energetically isolated from the high-energy bands. While the single-particle superlattice gaps vanish at the complete filling of the low-energy moiré Dirac bands, new Dirac points exist at Γ_s , as

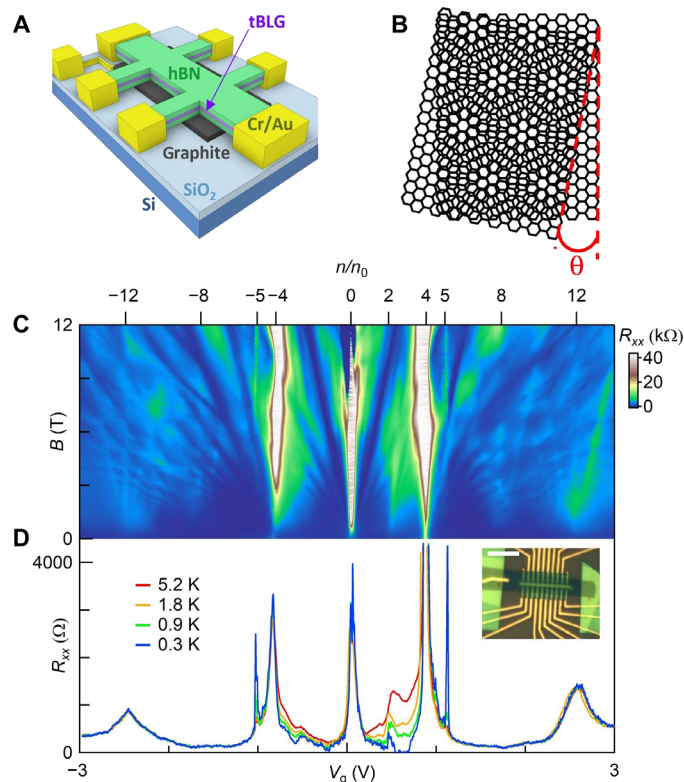


Fig. 1. Device geometry and magneto-transport data. (A) Schematic diagram of device geometry. (B) Schematic diagram of moiré superlattice formed by the twisted graphene layers. (C) R_{xx} versus magnetic field B and gate voltage V_g showing a Landau fan pattern. The top axis labels n_m , the number of charges per superlattice cell. (D) $R_{xx}(V_g)$ at different temperatures. Inset: Optical image of a tBLG device with a scale bar of $10 \mu\text{m}$.

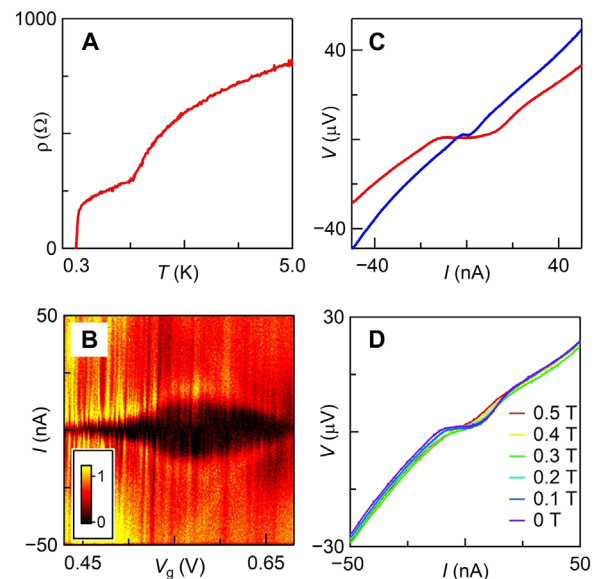


Fig. 2. Data from the superconducting state. (A) ρ versus temperature when the density is tuned to the superconducting phase ($V_g \sim 0.53$ V or $n_m \sim 2.5$). (B) Differential resistance dV/dI versus bias current and gate in the superconducting phase at base temperature (280 mK). Color scale is in units of kilohms. (C) Voltage-current characteristics at $T = 280$ mK and $V_g = 0.50$ V (blue) and 0.58 V (red), respectively. (D) V - I curves at different parallel magnetic fields.

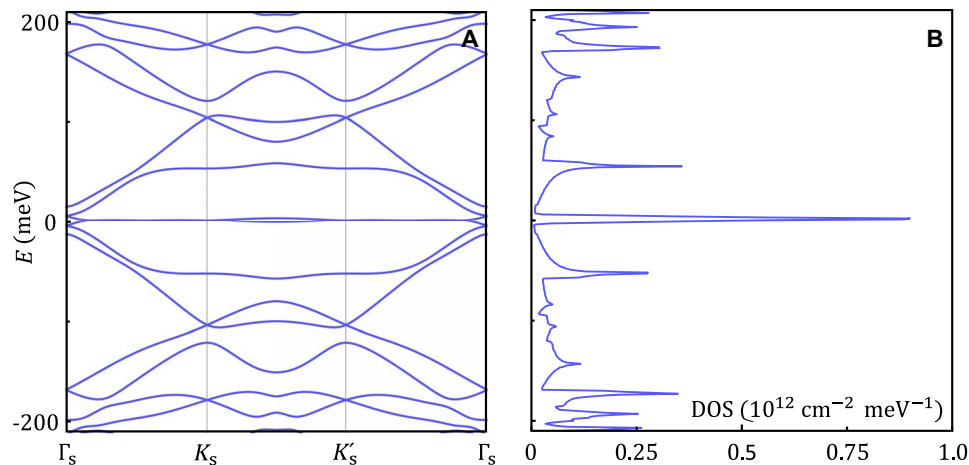


Fig. 3. Calculations of electronic band structures of 0.93° tBLG. (A) Energy dispersion. **(B)** DOS. In obtaining the DOS from the band structure, 1 meV was used for the energy interval, and the spin-valley degeneracy was considered.

shown in Fig. 3A. This explains why our R_{xx} peaks at $n_m = \pm 4$ are narrower compared to a previous report (8) and comparable to the one at the charge neutrality. The fact that the R_{xx} peak is relatively stronger at $n_m = 4$, together with the fact that superconductivity emerges only at the electron side, suggests that the electron-hole asymmetry is substantially enhanced by the electron-electron interactions. The emergence of both the Mott-like correlated insulating state at half-filling and the superconductivity at slightly higher doping indicates that, although the twist angle of 0.93° is ~15% smaller than the magic angle (7–9), the device hosts strongly correlated physics. This unexpected yet desirable behavior can also be understood by the calculated moiré bands and DOS of the 0.93° tBLG in Fig. 3. The low-energy moiré Dirac bands ($|n_m| < 4$) are bounded by the aforementioned multiple high-energy Dirac points near -4.68 and 5.96 meV. The narrow bandwidth (~11 meV), comparable to that of the magic angle tBLG (8, 9) and much smaller than the Coulomb interaction strength, produces a sharp DOS peak for $|n_m| < 4$.

We now turn to the behavior at large density ($|n_m| > 4$). At the lowest temperature, additional narrow resistance peaks are observed at $n_m = 5.08$ and -5.03 (Fig. 1C). Figure 4A shows a zoomed-in plot of the data for the $n_m = 5$ peaks. The peaks are almost indiscernible as T is increased above ~5 K. Plotting the resistance on an Arrhenius plot as shown in Fig. 4B yields an energy gap of ~1 K. These resistance peaks at $n_m = \pm 5$ have not been previously reported. Conceivably, it may arise from the presence of another domain with a slightly larger angle. Domains are likely to be present (35, 38, 39). However, the sharpness of the peaks and their small energy scale are very different from the behavior expected for a superlattice gap (8, 9), which are much broader and show very little low-temperature dependence. Thus, the peaks at $n_m \approx \pm 5$ are unlikely to originate from angular disorder. They are also unlikely to arise from a single-particle gap due to an alignment between hBN and graphene, because such a gap is expected to be ~100 K in magnitude (44, 45). We thus tentatively attribute these features to the emergence of a new correlated insulating state when the lowest (highest) high-energy conduction (valence) band is quarterly filled with electrons (holes). Evidently, in Fig. 3, our calculation reveals that these two bands are nearly flat in a large region of the moiré Brillouin zone, and that the corresponding DOS peaks are substantially large. From a background-subtracted $R_{xx}(V_g, B)$ plot, several Landau levels can be observed ema-

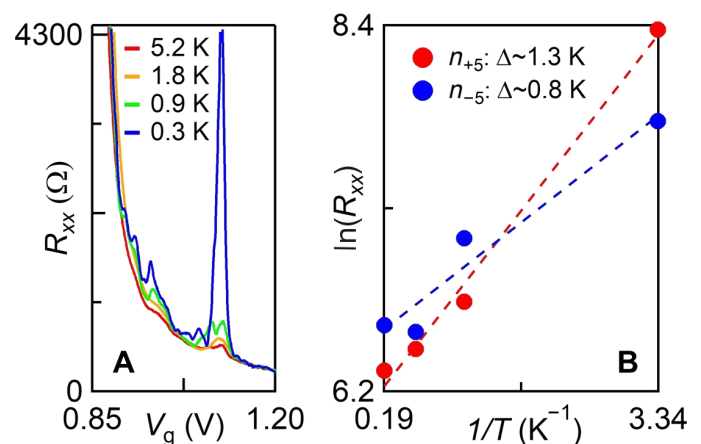


Fig. 4. Behavior of resistance peak near density $n_m = 5$. (A) Temperature dependence of the resistance peak. **(B)** Arrhenius plot of resistance showing a gap of ~0.1 meV.

nating from the two peaks and disperse toward the larger density sides, with degeneracy estimated to be 10 ± 2 , where the relatively large error bar of ± 2 arises from the limited range in magnetic field at which the features extrapolate to $n_m = \pm 5$ and $B = 0$. Hence, within error bars, the degeneracy measured is larger than the band degeneracy of 4. This unusual feature suggests that the fermionic quasi-particles not only respect the approximate spin-valley SU(4) symmetry but also might even enjoy an emergent new symmetry. More delicate future studies are required to examine the symmetries of these exotic insulating states and to determine whether or not they are quantum spin liquids.

Another unusual feature of the device behavior at high density is the presence of resistance peaks at $n_m = \pm 12$, where Landau fans with degeneracy of 4 emanate on both sides of each density. In addition, their maximum resistivities yield minimum conductivities $\sim 20e^2/h$. These features are reminiscent of the presence of Dirac points at the charge neutrality. Our moiré band structure calculation of the 0.93° tBLG reveals that a pair of Dirac points appears at K_s and K'_s near $n_m = \pm 12$ (Fig. 3). Consistently, the DOS calculation also shows local minima at the corresponding energies (Fig. 3).

CONCLUSION

In summary, in a twisted bilayer device at a small twist angle of 0.93° , superconductivity is observed near a Mott-like insulating state, with a critical temperature of 0.3 to 0.5 K. A gap is observed at a filling of ± 5 electrons per moiré unit cell. Theoretical calculations predict no band gap at this filling, indicating correlated insulating behavior for the quarter-filled high-energy band. Dirac points at a filling of ± 12 electrons per moiré unit cell lead to conductivity minima. Our work shows that electron correlations can markedly influence the properties of moiré superlattices even at small angles and high densities. Future work will focus on the spin-valley ordering of the insulating phases and investigations at lower temperatures to search for new superconducting phases, as well as theoretical efforts to understand the origin of these behaviors.

MATERIALS AND METHODS

Monolayer graphene, 5 to 10 nm of graphite, and 10 to 30 nm of hBN flakes were mechanically exfoliated onto SiO_2/Si wafers. Clean and homogeneously flat flakes were carefully identified. A dry transfer technique using PPC (polypropylene carbonate) on a PDMS (polydimethylsiloxane) point-contact stamp was used to transfer the flakes (40). A tear-and-stack method was used to twist the graphene layers relative to each other (2). After assembling the flakes, the stack was dropped onto a clean SiO_2/Si chip at 70° to 90°C to allow bubbles to flow away during the final lamination. Last, the temperature was raised to 120°C to melt the PPC onto the chip, which was then dissolved with acetone.

The stack was then shaped into a hall bar (channel width, $\sim 1\ \mu\text{m}$; leads separation, $\sim 1.5\ \mu\text{m}$) using electron beam lithography and reactive ion etching (RIE) with SF_6 and O_2 gases. One-dimensional electrical contact was made by patterning leads with electron beam lithography and depositing 2/50 nm of Cr/Au with electron beam deposition (40). A short O_2 RIE etch was done before deposition to improve contact (40).

Measurements were performed in pumped He^4 and He^3 refrigerators. Data were collected via standard ac and dc measurement techniques using SR830 lock-in amplifiers, Keithley 2400 source meters, and SR560 preamplifiers.

SUPPLEMENTARY MATERIALS

Supplementary material for this article is available at <http://advances.sciencemag.org/cgi/content/full/5/9/eaaw9770/DC1>

A. Theory of 0.93° Twisted Bilayer Graphene

B. Supplementary Data

Fig. S1. Extended electronic structures of the 0.93° tBLG.

Fig. S2. DOS versus density (n) for the 0.93° tBLG in fig. S1.

Fig. S3. Moiré band structures of the 0.93° tBLG in other models.

Fig. S4. Superconductivity response to magnetic field.

Fig. S5. Temperature dependence of the $n_m = -5$ resistance peak.

Fig. S6. Landau fan for $n_m = +5$.

REFERENCES AND NOTES

- J. M. B. Lopes, dos Santos, N. M. R. Peres, A. H. Castro Neto, Graphene bilayer with a twist: Electronic structure. *Phys. Rev. Lett.* **99**, 256802 (2007).
- Y. Cao, J. Y. Luo, V. Fatemi, S. Fang, J. D. Sanchez-Yamagishi, K. Watanabe, T. Taniguchi, E. Kaxiras, P. Jarillo-Herrero, Superlattice-induced insulating states and valley-protected orbits in twisted bilayer graphene. *Phys. Rev. Lett.* **117**, 116804 (2016).
- K. Kim, A. DaSilva, S. Huang, B. Fallahazad, S. Larentis, T. Taniguchi, K. Watanabe, B. J. LeRoy, A. H. MacDonald, E. Tutuc, Tunable moiré bands and strong correlations in small-twist-angle bilayer graphene. *Proc. Natl. Acad. Sci. U.S.A.* **114**, 3364–3369 (2017).
- F. Hu, S. R. Das, Y. Luan, T.-F. Chung, Y. P. Chen, Z. Fei, Real-space imaging of the tailored plasmons in twisted bilayer graphene. *Phys. Rev. Lett.* **119**, 247402 (2017).
- S. Carr, D. Massatt, S. Fang, P. Cazeaux, M. Luskin, E. Kaxiras, Twistronics: Manipulating the electronic properties of two-dimensional layered structures through their twist angle. *Phys. Rev. B* **95**, 075420 (2017).
- K. Kim, M. Yankowitz, B. Fallahazad, S. Kang, H. C. P. Movva, S. Huang, S. Larentis, C. M. Corbet, T. Taniguchi, K. Watanabe, S. K. Banerjee, B. J. LeRoy, E. Tutuc, van der Waals heterostructures with high accuracy rotational alignment. *Nano Lett.* **16**, 1989–1995 (2016).
- R. Bistritzer, A. H. MacDonald, Moiré bands in twisted double-layer graphene. *Proc. Natl. Acad. Sci. U.S.A.* **108**, 12233–12237 (2011).
- Y. Cao, V. Fatemi, A. Demir, S. Fang, S. L. Tomarken, J. Y. Luo, J. D. Sanchez-Yamagishi, K. Watanabe, T. Taniguchi, E. Kaxiras, R. C. Ashoori, P. Jarillo-Herrero, Correlated insulator behaviour at half-filling in magic-angle graphene superlattices. *Nature* **556**, 80–84 (2018).
- Y. Cao, V. Fatemi, S. Fang, K. Watanabe, T. Taniguchi, E. Kaxiras, P. Jarillo-Herrero, Unconventional superconductivity in magic-angle graphene superlattices. *Nature* **556**, 43–50 (2018).
- G. R. Stewart, Unconventional superconductivity. *Adv. Phys.* **66**, 75–196 (2017).
- M. Fidyrsiak, M. Zegrodnik, J. Spalek, Unconventional topological superconductivity and phase diagram for an effective two-orbital model as applied to twisted bilayer graphene. *Phys. Rev. B* **98**, 085436 (2018).
- T. Huang, L. Zhang, T. Ma, Antiferromagnetically ordered Mott insulator and $d+id$ superconductivity in twisted bilayer graphene: A quantum Monte Carlo study. *Sci. Bull.* **64**, 310–314 (2018).
- V. Kozii, H. Isobe, J. W. F. Venderbos, L. Fu, Nematic superconductivity stabilized by density wave fluctuations: Application to twisted bilayer graphene. *Phys. Rev. B* **99**, 144507 (2019).
- D. M. Kennes, J. Lischner, C. Karrasch, Strong correlations and $d+id$ superconductivity in twisted bilayer graphene. *Phys. Rev. B* **98**, 241407 (2018).
- C.-C. Liu, L.-D. Zhang, W.-Q. Chen, F. Yang, Chiral SDW and $d+id$ superconductivity in the magic-angle twisted bilayer-graphene. *Phys. Rev. Lett.* **121**, 217001 (2018).
- T. J. Peltonen, R. Ojajarvi, T. T. Heikkilä, Mean-field theory for superconductivity in twisted bilayer graphene. *Phys. Rev. B* **98**, 220504 (2018).
- H. C. Po, L. Zou, A. Vishwanath, T. Senthil, Origin of Mott insulating behavior and superconductivity in twisted bilayer graphene. *Phys. Rev. X* **8**, 031089 (2018).
- S. Ray, J. Jung, T. Das, Wannier Pairs in the superconducting twisted bilayer graphene and related systems. *Phys. Rev. B* **99**, 134515 (2019).
- B. Roy, V. Juričić, Unconventional superconductivity in nearly flat bands in twisted bilayer graphene. *Phys. Rev. B* **99**, 121407 (2019).
- C. Xu, L. Balents, Topological superconductivity in twisted multilayer graphene. *Phys. Rev. Lett.* **121**, 087001 (2018).
- J. W. F. Venderbos, R. M. Fernandes, Correlations and electronic order in a two-orbital honeycomb lattice model for twisted bilayer graphene. *Phys. Rev. B* **98**, 245103 (2018).
- F. Wu, A. H. MacDonald, I. Martin, Theory of phonon-mediated superconductivity in twisted bilayer graphene. *Phys. Rev. Lett.* **121**, 257001 (2018).
- M. Ochi, M. Koshino, K. Kuroki, Possible correlated insulating states in magic-angle twisted bilayer graphene under strongly competing interactions. *Phys. Rev. B* **98**, 081102 (2018).
- J. F. Dodaro, S. A. Kivelson, Y. Schattner, X. Q. Sun, C. Wang, Phases of a phenomenological model of twisted bilayer graphene. *Phys. Rev. B* **98**, 075154 (2018).
- Y.-Z. You, A. Vishwanath, Superconductivity from valley fluctuations and approximate SO (4) symmetry in a weak coupling theory of twisted bilayer graphene. *npj Quantum Mater.* **4**, 16 (2019).
- B. Lian, Z. Wang, B. A. Bernevig, Twisted bilayer graphene: A phonon driven superconductor. *Phys. Rev. Lett.* **122**, 257002 (2019).
- L. Rademaker, P. Mellado, Charge-transfer insulation in twisted bilayer graphene. *Phys. Rev. B* **98**, 235158 (2018).
- X. Y. Xu, K. T. Law, P. A. Lee, Kekulé valence bond order in an extended Hubbard model on the honeycomb lattice with possible applications to twisted bilayer graphene. *Phys. Rev. B* **98**, 121406 (2018).
- A. Thomson, S. Chatterjee, S. Sachdev, M. S. Scheurer, Triangular antiferromagnetism on the honeycomb lattice of twisted bilayer graphene. *Phys. Rev. B* **98**, 075109 (2018).
- H. C. Po, L. Zou, T. Senthil, A. Vishwanath, Faithful tight-binding models and fragile topology of magic-angle bilayer graphene. *Phys. Rev. B* **99**, 195455 (2018).
- L. Chen, H.-Z. Li, R.-S. Han, Magnetic-impurity resonance states for different pairing symmetries in twisted bilayer graphene. *J. Phys. Condens. Matter* **31**, 065601 (2018).
- B. Padhi, C. Setty, P. W. Phillips, Doped twisted bilayer graphene near magic angles: Proximity to wigner crystallization, not mott insulation. *Nano Lett.* **18**, 6175–6180 (2018).
- H. M. Guo, X. C. Zhu, S. P. Feng, R. T. Scalettar, Pairing symmetry of interacting fermions on a twisted bilayer graphene superlattice. *Phys. Rev. B* **97**, 235453 (2018).

34. P. Lucignano, D. Alf , V. Cataudella, D. Ninno, G. Cantele, The crucial role of atomic corrugation on the flat bands and energy gaps of twisted bilayer graphene at the "magic angle" $0\text{--}1.08^\circ$. *Phys. Rev. B* **99**, 195419 (2019).
35. M. Yankowitz, S. Chen, H. Polshyn, Y. Zhang, K. Watanabe, T. Taniguchi, D. Graf, A. F. Young, C. R. Dean, Tuning superconductivity in twisted bilayer graphene. *Science* **363**, 1059–1064 (2019).
36. Y. Cao, D. Chowdhury, D. Rodan-Legrain, O. Rubies-Bigord , K. Watanabe, T. Taniguchi, T. Senthil, P. Jarillo-Herrero, Strange metal in magic-angle graphene with near Planckian dissipation. arXiv:1901.03710 [cond-mat] (11 January 2019).
37. A. L. Sharpe, E. J. Fox, A. W. Barnard, J. Finney, K. Watanabe, T. Taniguchi, M. A. Kastner, D. Goldhaber-Gordon, Emergent ferromagnetism near three-quarters filling in twisted bilayer graphene. *Science* **365**, 605–608 (2019).
38. Y. Choi, Jeannette Kemmer, Y. Peng, A. Thomson, H. Arora, R. Polski, Y. Zhang, H. Ren, J. Alicea, G. Refael, Felix von Oppen, K. Watanabe, T. Taniguchi, S. Nadj-Perge, Imaging electronic correlations in twisted bilayer graphene near the magic angle. arXiv:1901.02997 [cond-matmes-hall] (10 January 2019).
39. A. Kerelsky, L. McGilly, D. M. Kennes, L. Xian, M. Yankowitz, S. Chen, K. Watanabe, T. Taniguchi, J. Hone, C. Dean, A. Rubio, A. N. Pasupathy, Magic angle spectroscopy. *Nature* **572**, 95–100 (2019).
40. L. Wang, I. Meric, P. Y. Huang, Q. Gao, Y. Gao, H. Tran, T. Taniguchi, K. Watanabe, L. M. Campos, D. A. Muller, J. Guo, P. Kim, J. Hone, K. L. Shepard, C. R. Dean, One-dimensional electrical contact to a two-dimensional material. *Science* **342**, 614–617 (2013).
41. B. Hunt, J. D. Sanchez-Yamagishi, A. F. Young, M. Yankowitz, B. J. LeRoy, K. Watanabe, T. Taniguchi, P. Moon, M. Koshino, P. Jarillo-Herrero, R. C. Ashoori, Massive Dirac fermions and Hofstadter butterfly in a van der Waals heterostructure. *Science* **340**, 1427–1430 (2013).
42. G. H. Wannier, A result not dependent on rationality for Bloch electrons in a magnetic field. *Phys. Status Solidi* **88**, 757–765 (1978).
43. M. Koshino, N. F. Q. Yuan, T. Koretsune, M. Ochi, K. Kuroki, L. Fu, Maximally localized Wannier orbitals and the extended hubbard model for twisted bilayer graphene. *Phys. Rev. X* **8**, 031087 (2018).
44. L. A. Ponomarenko, R. V. Gorbachev, G. L. Yu, D. C. Elias, R. Jalil, A. A. Patel, A. Mishchenko, A. S. Mayorov, C. R. Woods, J. R. Wallbank, M. Mucha-Kruczynski, B. A. Piot, M. Potemski, I. V. Grigorieva, K. S. Novoselov, F. Guinea, V. I. Fal'ko, A. K. Geim, Cloning of Dirac fermions in graphene superlattices. *Nature* **497**, 594–597 (2013).
45. C. R. Dean, L. Wang, P. Maher, C. Forsythe, F. Ghahari, Y. Gao, J. Katoch, M. Ishigami, P. Moon, M. Koshino, T. Taniguchi, K. Watanabe, K. L. Shepard, J. Hone, P. Kim, Hofstadter's butterfly and the fractal quantum Hall effect in moir  superlattices. *Nature* **497**, 598–602 (2013).

Acknowledgments: F.Z. is grateful to F. Wu, A. Po, and F. Yang for valuable discussions. We thank the groups of J. Hone and C. Dean for experimental advice on device fabrication.

Funding: The experiments are supported by the DOE BES Division under grant no. ER 46940-DE-SC0010597. S.C. acknowledges partial support from the Center for Emergent Materials: an NSF MRSEC under award number DMR-1420451 for device fabrication in NSL. The theoretical works (Q.W. and F.Z.) are supported by the Army Research Office under grant number W911NF-18-1-0416. Growth of hBN crystals was supported by the Elemental Strategy Initiative conducted by the MEXT, Japan and a Grant-in-Aid for Scientific Research on Innovative Areas "Science of Atomic Layers" from JSPS. **Author contributions:** M.B. and C.N.L. conceived the experiment. T.T. and K.W. synthesized the hBN crystals. E.C. fabricated the samples. R.K. assisted with sample preparation. E.C. and S.C. performed the transport measurements. H.T., R.L., and S.T. assisted with fabrication and measurements. Q.W. and F.Z. performed the theoretical calculations. E.C., Q.W., S.C., F.Z., M.B., and C.N.L. analyzed and interpreted the data. E.C., F.Z., M.B., and C.N.L. wrote the manuscript. All authors discussed and commented on the manuscript. **Competing interests:** The authors declare that they have no competing interests. **Data and materials availability:** All data needed to evaluate the conclusions in the paper are present in the paper and/or the Supplementary Materials. Additional data related to this paper may be requested from the authors. The devices can be provided by Lau and Bockrath groups pending scientific review and a completed material transfer agreement and subject to availability. Requests for devices should be submitted to lau.232@osu.edu or bockrath.31@osu.edu.

Submitted 13 February 2019

Accepted 29 August 2019

Published 27 September 2019

10.1126/sciadv.aaw9770

Citation: E. Codecido, Q. Wang, R. Koester, S. Che, H. Tian, R. Lv, S. Tran, K. Watanabe, T. Taniguchi, F. Zhang, M. Bockrath, C. N. Lau, Correlated insulating and superconducting states in twisted bilayer graphene below the magic angle. *Sci. Adv.* **5**, eaaw9770 (2019).

Correlated insulating and superconducting states in twisted bilayer graphene below the magic angle

Emilio Codecido, Qiyue Wang, Ryan Koester, Shi Che, Haidong Tian, Rui Lv, Son Tran, Kenji Watanabe, Takashi Taniguchi, Fan Zhang, Marc Bockrath and Chun Ning Lau

Sci Adv **5** (9), eaaw9770.
DOI: 10.1126/sciadv.aaw9770

ARTICLE TOOLS

<http://advances.sciencemag.org/content/5/9/eaaw9770>

SUPPLEMENTARY MATERIALS

<http://advances.sciencemag.org/content/suppl/2019/09/23/5.9.eaaw9770.DC1>

REFERENCES

This article cites 43 articles, 6 of which you can access for free
<http://advances.sciencemag.org/content/5/9/eaaw9770#BIBL>

PERMISSIONS

<http://www.sciencemag.org/help/reprints-and-permissions>

Use of this article is subject to the [Terms of Service](#)

Science Advances (ISSN 2375-2548) is published by the American Association for the Advancement of Science, 1200 New York Avenue NW, Washington, DC 20005. 2017 © The Authors, some rights reserved; exclusive licensee American Association for the Advancement of Science. No claim to original U.S. Government Works. The title *Science Advances* is a registered trademark of AAAS.